Int. J. Environ. Sci. Technol. (2016) 13:423–434
DOI 10.1007/s13762-015-0907-x

ORIGINAL PAPER

Synthesis of a novel 3 %Ru/$CeZr_{0.5}GdO_4$ nanocatalyst and its application in the dry and steam reforming of methane

Z. Shariatinia[1] · **Y. Khani**[1] · **F. Bahadoran**[2]

Received: 3 April 2015 / Revised: 13 September 2015 / Accepted: 8 October 2015 / Published online: 19 October 2015

Abstract A novel 3 %Ru/$CeZr_{0.5}GdO_4$ nanocatalyst was synthesized by the wet impregnation method and evaluated for its catalytic activity in dry and steam reforming of methane at atmospheric pressure, seven various temperatures (from 500 to 800 °C) and two different gas hourly space velocity values (7000, 10,500 h^{-1}). The thermogravimetric diagrams of the used catalysts did not illustrate any carbon deposition on the catalysts applied in both the dry and steam reforming processes and this valuable phenomenon was supported by the scanning electron microscopy images. The low onset reduction temperature in the temperature-programmed reduction profile of the 3 %Ru/$CeZr_{0.5}GdO_4$ at 183.21 °C reflected much convenient reducibility/oxygen mobility property of the catalyst. Comparing the CH_4 conversions in the dry reforming (92 %) and steam reforming (97 %) reactions using the gas hourly space velocity = 10,500 h^{-1} at 800 °C indicated higher efficiency of the steam reforming process. The time on stream experiments for the dry and steam reforming reactions exhibited that the CH_4 and CO_2 conversions are almost constant (and even they are slightly increased in the dry reforming) after 30 h reflecting the catalyst outstanding stability with time, absence of coke deposition and catalyst very high activity.

Keywords Methane dry reforming · Methane steam reforming · $CeZr_{0.5}GdO_4$ support · Nanocatalyst

Introduction

Nowadays, the dry reforming of methane [DRM, Eq. (1)] has attracted much attention due to its valuable environmental benefits including biogas utilization (Kohn et al. 2014; Lucredio et al. 2012), removal of two green house gasses (methane and carbon dioxide) and conversion of natural gas with a high carbon dioxide content to valuable syngas (CO, H_2) (Lunsford 2000). The DRM reaction produces a low syngas ratio ($H_2/CO = 1$), which is appropriate for the synthesis of oxygenated chemicals (Wurzel et al. 2000) and hydrocarbons from Fischer–Tropsch synthesis (Oyama et al. 2012). Syngas from DRM can also be used to store solar or nuclear energy (Levy et al. 1992) through the chemical energy transmission system. Solar energy can convert feed gases (CH_4 and CO_2) to syngas that can be exported to places where energy sources are limited. The energy stored in syngas is liberated by the backward reaction and utilized as an energy source. On the other hand, for any catalytic system, the DRM reaction is accompanied by fast side-reactions which reduce the selectivity such as the reverse water–gas shift reaction (Eq. 2). In addition to more common problems in high-temperature catalysis, such as active particle sintering, DRM catalysts typically suffer from carbon deposition due to the high C/H ratio of the feedstock. The CO disproportionation (the Boudouard reaction) (Eq. 3) and

---

Electronic supplementary material The online version of this article (doi:10.1007/s13762-015-0907-x) contains supplementary material, which is available to authorized users.

✉ Z. Shariatinia
shariati@aut.ac.ir

[1] Department of Chemistry, Amirkabir University of Technology (Tehran Polytechnic), P. O. Box: 15875-4413, Tehran, Iran

[2] Gas Research Division, Research Institute of Petroleum Industry, West Blvd. of Azadi Sport Complex, Tehran 1485733111, Iran

methane decomposition (Eq. 4) are the main surface carbon forming processes.

$$CH_4 + CO_2 \rightarrow 2CO + 2H_2 \qquad \Delta H^0_{298} = +247\ \text{kJ/mol} \tag{1}$$

$$CO_2 + H_2 \rightarrow CO + H_2O \qquad \Delta H^0_{298} = +41.17\ \text{kJ/mol} \tag{2}$$

$$2CO \rightarrow CO_2 + C(s) \qquad \Delta H^0 = -171\ \text{kJ/mol} \tag{3}$$

$$CH_4 \rightarrow 2H_2 + C(s) \qquad \Delta H^0 = +75\ \text{kJ/mol} \tag{4}$$

Nickel-based catalysts have been shown to be highly active for the DRM reaction, but are generally less resistant to carbon deposition. Their stability can be improved by maintaining small supported nickel nanoparticles (Quek et al. 2010) using metal–support interactions to reduce sintering. This includes strong metal–support interaction effects, which could have the additional reactive benefit of inhibiting the adsorptivity of DRM reaction products.

The steam reforming of methane (SRM, Eqs. 5–7) is the preferred way of producing syngas that can be used for chemical, fuel and power production (Jakobsen et al. 2010). Traditionally, nickel-based catalysts are used for the SRM process in numerous industrial applications. However, it is required to develop other SRM catalysts that are able to operate at low steam/carbon ratios. The nickel catalysts form carbon whiskers that will eventually destroy the catalysts (Bakkerud 2005). One solution to this problem is the utilization of noble metal catalysts such as Ru, Rh, Ir, Pt and Pd which are more resistant against the formation of carbon whiskers (Rostrup-Nielsen and Hansen 1993). It was indicated that Ru is among the most active metals for catalyzing the SRM reaction (Jones et al. 2008; Rostrup-Nielsen and Hansen 1993). Other noble metals such as Rh, Pt, Pd and Ir also revealed good SRM activity although different relative reactivities were observed (Jones et al. 2008; Wei and Iglesia 2004).

$$CH_4 + H_2O \rightarrow CO + 3H_2 \qquad \Delta H^0_{298} = +206.1\ \text{kJ/mol} \tag{5}$$

$$CO + H_2O \rightarrow CO_2 + H_2 \qquad \Delta H^0_{298} = -41.17\ \text{kJ/mol} \tag{6}$$

$$CH_4 + 2H_2O \rightarrow CO_2 + 4H_2 \qquad \Delta H^0_{298} = +165.0\ \text{kJ/mol} \tag{7}$$

In this research, a novel 3 %Ru/$CeZr_{0.5}GdO_4$ nanocatalyst was synthesized and applied in the DRM and SRM reactions in order to find a desired catalyst with improved catalytic activity and reduced carbon deposition on its surface compared with the commonly used catalysts. Surprisingly, successful results were obtained in these experiments so that high conversions and yields were gained using the synthesized catalyst. Moreover, the absence of coke deposition on the catalyst surface was evidenced by thermogravimetric analysis (TGA) and field-emission scanning electron microscopy (FE-SEM) micrographs. The results can be ascribed to the synergistic effects of spinel $CeZr_{0.5}GdO_4$ support and Ru active metal leading to efficient support–metal interaction that prevents the catalyst sintering/deactivation. The 3 %Ru/$CeZr_{0.5}GdO_4$ nanocatalyst with very high catalytic activity and extremely much stability against coke formation thus can be proposed and utilized for the methane reforming reactions to achieve high conversions/yields. This study was a cooperation work performed at both Department of Chemistry, Amirkabir University of Technology (Tehran Polytechnic), and Gas Research Division, Research Institute of Petroleum Industry, Tehran, Iran, in 2014.

Materials and methods

Materials

All materials were purchased from Sigma-Aldrich and Merck companies and were used as received. They were zirconium(IV) oxynitrate hydrate ($ZrO(NO_3)_2{\cdot}xH_2O$, 99 %), cerium nitrate hexahydrate ($Ce(NO_3)_3{\cdot}6H_2O$, 99 %), gadolinium nitrate hexahydrate ($Gd(NO_3)_3{\cdot}6H_2O$, 99.99 %), ruthenium nitrosyl nitrate ($Ru^{III}(N{=}O)(NO_3)_3$, in diluted nitric acid, containing ~1.5 % Ru), ammonium hydroxide (NH_4OH, 28 % NH_3 in H_2O, ≥99.99 %) and glycerin ($OHCH_2CH(OH)CH_2OH$, ≥99.5 %).

Synthesis of support and nanocatalyst

The $CeZr_{0.5}GdO_4$ support was synthesized according to a gel combustion technique. For this purpose, a solution of $Ce(NO_3)_3{\cdot}6H_2O$, $ZrO(NO_3)_2{\cdot}xH_2O$ and $Gd(NO_3)_3{\cdot}6H_2O$ with a 1:0.5:1 molar ratio was prepared in distilled water to which a solution of glycerin was added as a fuel so that the molar ratio of metals/fuel was 2.5:20. The pH of the solution was adjusted to 12 using NH_4OH solution. Then, the suspension was heated up to 80 °C, and the mixture was stirred for about 12 h in order to become concentrated by evaporation of water. The concentrated gel was calcined in a furnace for 10 h at 800 °C with a heating rate of 2 °C/min.

Synthesis of 3 %Ru nanocatalyst on $CeZr_{0.5}GdO_4$ support was performed by the wet impregnation method. An appropriate amount of $Ru^{III}(N{=}O)(NO_3)_3$ solution was added to the $CeZr_{0.5}GdO_4$ support followed by overnight drying at 120 °C and then calcination at 700 °C for 2 h with a heating rate of 2 °C/min.

Characterization of support and nanocatalyst

To identify the phases and crystallinities of samples, X-ray diffraction (XRD) analysis was obtained with an INEL EQUINOX 3000 X-ray diffractometer using Cu K_α radiation ($\lambda = 1.5406$ Å) in the 2θ range of 5°–110°. The phases were determined using Joint Committee on Powder Diffraction Standard (JCPDS) files. The surface area, pore volume and pore diameters were estimated by BET (Brunauer–Emmett–Teller) method from nitrogen adsorption–desorption isotherms data obtained at −196 °C on a constant-volume adsorption apparatus (QuantaChrome, NOVA2000). Prior to the adsorption–desorption measurements, all the samples were degassed at 200 °C in the N_2 flow for 3 h. The FE-SEM micrographs were taken from Philips (XL30) and Zeiss instruments, under vacuum, accelerated at 10 and 15 kV, respectively.

Amounts of carbon deposited on the surfaces of used catalysts were evaluated by thermogravimetric analysis (TGA) and differential thermal analysis (DTA) in an air atmosphere with a heating rate of 10 °C/min up to 800 °C on a TG–DTA SDTA 851e instrument. The Fourier transform infrared (FT-IR) spectra of the used nanocatalysts were collected on a Bruker Vertex 80 spectrometer in the region of 400–4000 cm^{-1} for addressing surface functional groups.

The bulk temperature-programmed reduction (TPR) behavior of the catalyst was studied using a BELCAT-A system; 0.05 g of the catalyst was initially heated under a helium flow (40 NmL/min) at a rate of 10 °C/min to 200 °C for 20 min. Then, the reducing gas (5 % H_2 in Ar) was switched on at 50 NmL/min and the temperature was raised at a rate of 10 °C/min until it was reached 700 °C. The effluent gas was passed through a cooling trap (at a temperature lower than −50 °C) to condense and collect water generated during the reduction process. A thermal conductivity detector (TCD) was used to determine the amount of H_2 consumed.

Catalytic activity experiments

The catalytic reforming of methane was carried out under atmospheric pressure in a flow system equipped with a 6-mm ID fixed bed quartz reactor and an electrically heating furnace. The flow rates of gases were controlled by a mass flow controller (MFC, Brooks 5850E); 0.25 g of each nanocatalyst (mesh size 20–40 for DRM and 60–80 for SRM reaction) was loaded in the reactor. The catalyst was pretreated for 2 h at 700 °C in a stream of 1:3 H2/Ar for activation of 3 %Ru/$CeZr_{0.5}GdO_4$ prior to the catalytic reforming reactions.

In the DRM reaction, methane and carbon dioxide (as feeds) with Ar as a diluent (in 1:1:3 molar ratio) were used. In the SRM reaction, the optimum H_2O/CH_4 ratio of 3 was selected for the catalytic reaction experiments and a mixture of $H_2O/CH_4/Ar$ (mole ratio of 3:1:3) was used as a feed. In the SRM reaction, water was pumped at a constant flow rate to the evaporator using a HPLC pump (Eldex Laboratories, Model pN: 5935-optos, pump 2 SMP) and the generated steam was mixed with the reaction mixture.

Two gas hourly space velocity (GHSV) values of 7000 and 10,500 h^{-1} (equal to WHSV = 2 and 3 L/h) were applied for the feed in the reforming reactions. The reaction was performed under atmospheric pressures at seven various temperatures (500, 550, 600, 650, 700, 750 and 800 °C). The compositions of the streams (reactants and products) were determined by an on-line three-channel gas chromatograph (Varian 3800 equipped with two TCD and one FID detectors). The CH_4, CO_2 conversions (X_{CH4} and X_{CO2}), CO, H_2 yields (Y_{CO} and Y_{H2}) and H_2/CO ratio for the DRM reaction were calculated from the following Eqs. (8)–(12) (Bachiller-Baeza et al. 2013; Bermúdez et al. 2012; Zhai et al. 2011).

$$X_{CH_4}(\%) = \frac{[CH_4]in - [CH_4]out}{[CH_4]in} \times 100 \tag{8}$$

$$X_{CO_2}(\%) = \frac{[CO_2]in - [CO_2]out}{[CO_2]in} \times 100 \tag{9}$$

$$Y_{CO}(\%) = \frac{[CO]out}{[CH_4]in + [CO_2]in} \times 100 \tag{10}$$

$$Y_{H_2}(\%) = \frac{[H_2]out}{2 \times [CH_4]in} \times 100 \tag{11}$$

$$\frac{H_2}{CO}\text{ratio} = \frac{\text{mol of } H_2 \text{ produced}}{\text{mol of CO produced}} \tag{12}$$

The CO and H_2 yields (Y_{CO} and Y_{H2}) for the SRM reaction were calculated from the following Eqs. (13) and (14) (Roy et al. 2014). The CH_4 conversion (X_{CH4}) and H_2/CO ratio were calculated by Eqs. (8) and (12).

$$Y_{CO}(\%) = \frac{[CO]out}{[CO]out + [CO_2]out} \times 100 \tag{13}$$

$$Y_{H_2}(\%) = \frac{[H_2]out}{[CH_4]in} \times 100 \tag{14}$$

Results and discussion

Characterization of support and nanocatalyst

In order to evaluate the surface areas and pore volumes of the synthesized $CeZr_{0.5}GdO_4$ support and 3 %Ru/$CeZr_{0.5}GdO_4$ nanocatalyst, their nitrogen physisorption data were obtained at 77 K. Figure S1 indicates that the N_2 adsorption/desorption isotherms of the two samples are similar and each of them contains a broad hysteresis loop at a relative pressure of ~0.5–0.9. From the literature, it is well known that this shape for the adsorption/desorption isotherms belongs to the type IV isotherm with an obvious hysteresis loop at high relative pressures reflecting the existence of mesopores. The textural data listed in Table 1 also confirm the formation of mesoporous structures. The pore size distributions for the fresh $CeZr_{0.5}GdO_4$ support and 3 %Ru/$CeZr_{0.5}GdO_4$ catalyst displayed in Fig. S2 are also comparable indicating Gaussian shape distributions for the pore sizes.

It is seen in Table 1 that the specific surface area and pore volume of the support are decreased upon impregnation of 3 %Ru catalyst. In fact, it is expected that the impregnation of the active metal leads to reduction in the surface area and pore volume due to filling the surface/pores of support by the metal catalyst. Similarly, it was indicated that aqueous impregnation of modifiers led to a certain reduction in the surface area of a Ni–Al_2O_3 catalyst (Luna and Iriarte 2008).

The FE-SEM micrographs of the $CeZr_{0.5}GdO_4$ support as well as 3 %Ru/$CeZr_{0.5}GdO_4$ catalyst were taken to get insight about their surface morphology and particle size. The FE-SEM images in Fig. 1a, b exhibit the sheet-like morphology for the $CeZr_{0.5}GdO_4$ support but for the 3 %Ru/$CeZr_{0.5}GdO_4$, it is obviously seen that the metallic Ru particles (that are near 80 nm in size) are dispersed on the surface of the $CeZr_{0.5}GdO_4$ support.

The XRD patterns of the $CeZr_{0.5}GdO_4$ support and fresh 3 %Ru/$CeZr_{0.5}GdO_4$ catalyst are illustrated in Fig. 1c, d. The sharpest peak for the $CeZr_{0.5}GdO_4$ support is observed at $2\theta = 27.75°$ (intensity = 100 %) and other sharp peaks appear at $2\theta = 32.61°$, 47.88°, 57.57° and 78.53°. The characteristic peaks of CeO_2, ZrO and Gd_2O_3 are also observed within the XRD pattern of the $CeZr_{0.5}GdO_4$ indicating the presence of these metals, but there are additional peaks reflecting the specific XRD pattern for this new material. The XRD pattern of the 3 %Ru/$CeZr_{0.5}GdO_4$ nanocatalyst reveals the characteristic sharp peaks of the support on which Ru has been impregnated (the corresponding peaks of the active metal Ru are detectable).

The full-width at half-maximum (FWHM) corresponding to the sharpest 2θ positions in the XRD patterns was used to determine the average crystallite size using the Debye–Scherrer equation ($d = 0.9\ \lambda/\beta \cos\theta$) (Klug and Alexander 1954) where d is the average crystallite size, λ is the X-ray wavelength, β is the FWHM and θ is the diffraction angle. The average crystallite sizes measured from the XRD diagrams for the $CeZr_{0.5}GdO_4$ support and 3 %Ru/$CeZr_{0.5}GdO_4$ catalyst are 201.8 and 135.1 nm, respectively. The sizes calculated from the XRD diffractograms are very much larger than those measured from the BET analysis and this may be due to the agglomeration of particles when they are prepared for the XRD analysis.

The TPR analysis was performed to find the reduction temperature of the 3 %Ru/$CeZr_{0.5}GdO_4$ catalyst (Fig. 1e). It is seen that there is one sharp peak at 183.21 °C that has been appeared at a low temperature compared with those of the catalysts reported in literature (Barroso-Quiroga and Castro-Luna 2010; Yang et al. 2010). The peak at 183.21 °C for the 3 %Ru/$CeZr_{0.5}GdO_4$ catalyst can be assigned to the reduction of segregated Ru_2O_3 (or Ru^{III}) to metallic Ru^0. Comparing this reduction temperature with those of other reported catalysts, it is found that the 3 %Ru/$CeZr_{0.5}GdO_4$ catalyst is exceptionally conveniently reduced. For example, the reduction temperatures of the promoted catalysts using La_2O_3 and CeO_2 including 10 %Ni/γ-Al_2O_3, 10 %Ni/3 %La_2O_3-γ-Al_2O_3 and 10 %Ni/3 %CeO_2–3 %La_2O_3-γ-Al_2O_3 were measured at about 800 °C (Yang et al. 2010). Also, the TPR profiles of various Ni/γ-Al_2O_3 catalysts including Kaiser A201, Kaiser A202 and Rhône Poulenc exhibited two and three peaks near 700, 1100–1200 and 700, 900, 1100 K, respectively (Barroso-Quiroga and Castro-Luna 2010). The H_2-TPR results for Ni-doped La_2O_3 catalysts indicated the reduction temperatures near 350 °C (Sutthiumporn and Kawi 2011). Similarly, it was shown that the reduction temperatures of $Ce_{0.75}Zr_{0.25}O_2$ (CZ)-supported Ru catalysts were appeared between 473 and 523 K, and compared with CZ support, no reduction peaks were observed at about 940 K in the traces of the Ru catalysts (Chen et al. 2010). For the Ru-based catalysts, no reduction peak at about 940 K indicated that contribution of Ru species facilitated the reduction of surface (or subsurface) oxygen and some bulk lattice oxygen species. This effect was attributed to the spillover of hydrogen species from metallic Ru particles to

Table 1 Textural properties of the support and fresh nanocatalyst

Sample	BET surface area (m^2/g)	Total pore volume (cm^3/g)	Micropore volume (cm^3/g)	Mesopore volume (cm^3/g)	Pore size (nm)	Particle size (nm)
$CeZr_{0.5}GdO_4$	162.47	0.2132	0.0023	0.2109	6.88	51.22
3 %Ru/$CeZr_{0.5}GdO_4$	90.40	0.2015	0.0019	0.1996	8.56	66.37

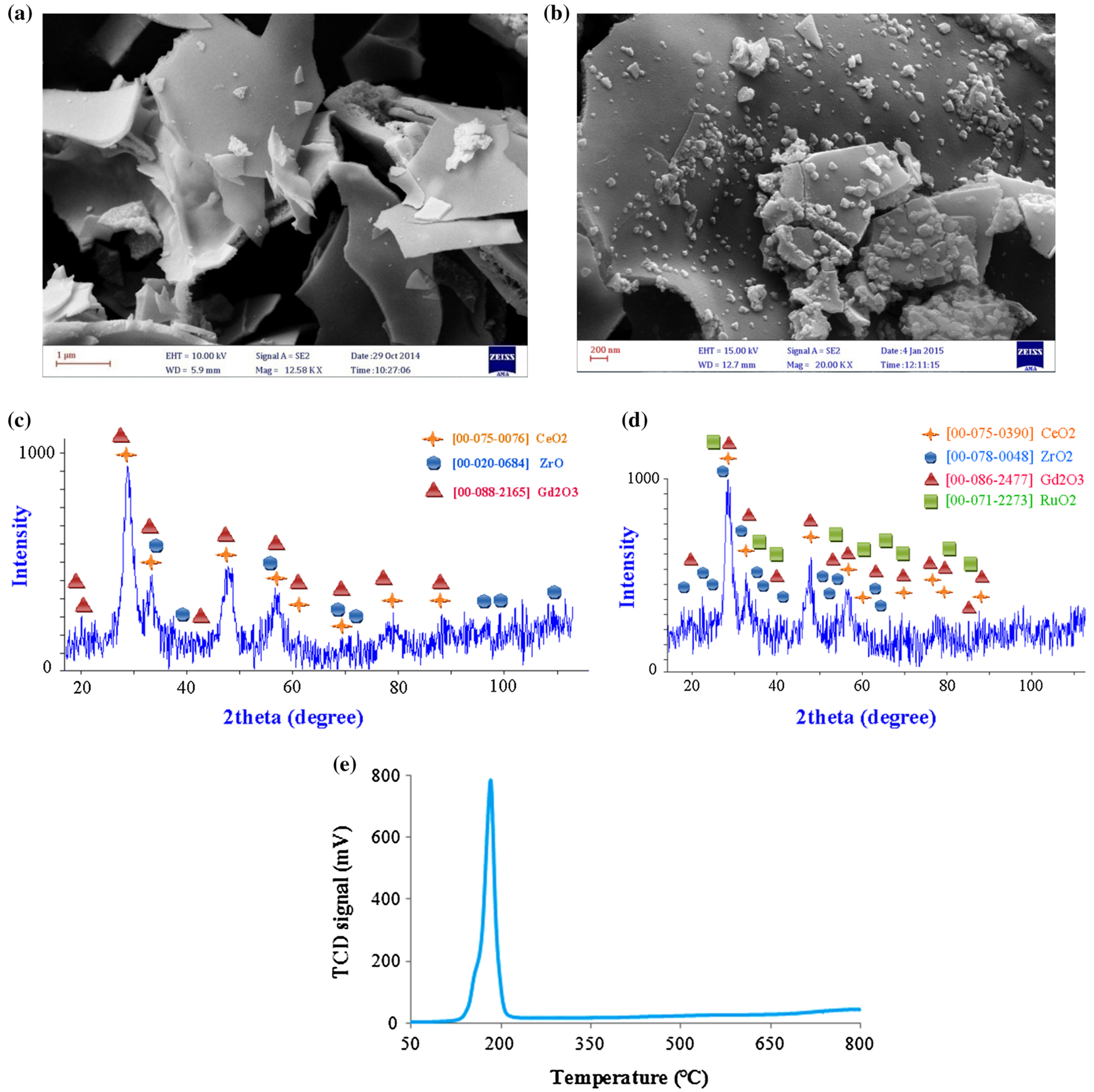

Fig. 1 FE-SEM micrographs of fresh **a** $CeZr_{0.5}GdO_4$ support and **b** 3 %Ru/$CeZr_{0.5}GdO_4$ nanocatalyst. The XRD patterns of fresh **c** $CeZr_{0.5}GdO_4$ support and **d** 3 %Ru/$CeZr_{0.5}GdO_4$ catalyst. **e** The TPR curve of 3 %Ru/$CeZr_{0.5}GdO_4$ catalyst

the CZ support. In addition, the formed metallic Ru perhaps reduced the support metal oxides (Chen et al. 2010).

Although the reason for the reduction has not yet been identified exactly, the most probable explanation is that the hydrogen molecules can only consume the oxygen molecules located on the surface of catalyst. As a result, the positions and intensities of the H_2 consumption peaks could be used to reveal the surface oxygen mobility of the catalyst. The lower the temperature at which the reduction peak appears, the higher the oxidizing ability/oxygen mobility of a metal oxide is (Sun et al. 2008; Wu and Kawi 2009). Therefore, the low onset reduction temperature for our catalyst suggests that it has high oxygen mobility on its surface. Comparing the TPR profile of 3 %Ru/$CeZr_{0.5}GdO_4$ catalyst with that of 10 %Ni/γ-Al_2O_3 reported in literature (Barroso-Quiroga and Castro-Luna 2010; Yang et al. 2010) confirms that the nature of support also plays a key role on the amount of surface oxygen mobility.

The effect of surface oxygen mobility on preventing the catalyst deactivation was investigated using Sr-doped Ni–La_2O_3 catalyst in the DRM reaction (Sutthiumporn and Kawi 2011). The low carbon deposition over the catalyst surface was described as the existence of a high amount of lattice oxygen species on the catalyst surface which promoted C–H activation resulting in high H_2 production. Furthermore, it was suggested that these surface oxygen species might adsorb CO_2 molecules to form bidentate carbonate species that could react with the deposited surface carbon compounds created during the DRM reaction leading to higher CO_2 conversion and lower carbon formation.

It is notable that the onset reduction temperature in the $CeZr_{0.5}GdO_4$-supported 3 %Ru catalyst is very low and this is an appropriate result for the catalyst regeneration. From the TPR result, it can be concluded that the nature of support strongly influences the reducibility of catalyst. Consequently, it may be expected that the 3 %Ru/$CeZr_{0.5}GdO_4$ catalyst with the reduction peak at a low temperature will present high catalytic activity.

Catalytic activities in the DRM and SRM reactions

The DRM and SRM reactions

The catalytic performance of the 3 %Ru/$CeZr_{0.5}GdO_4$ nanocatalyst was evaluated in the DRM and SRM reactions using two feed GHSVs = 7000, 10,500 h^{-1} (equal to WHSV = 2, 3 L/h) under P = 1 atm and at seven various temperatures (500, 550, 600, 650, 700, 750 and 800 °C). Comparing the CH_4, CO_2 conversions, H_2 yields and H_2/CO ratios at the different GHSVs (Figs. 2, 3) illustrates that the best results were found at the GHSV = 7000 h^{-1}. As expected, it was indicated that all of the conversions and yields were reduced by increasing the GHSV value that is related to faster coke formation on the catalyst at higher GHSV. For example, the CH_4 conversions in the DRM reaction using feed WHSV = 2, 3 L/h at 800 °C are 91.78, 86.86 % and the CO_2 conversions are 89.12, 83.80 %, respectively. It is also obvious from the diagrams that raising the reaction temperature from 500 to 800 °C results in increasing the conversions and yields.

In the DRM reaction, the CH_4 conversions are lower than their corresponding CO_2 conversions (Figs. 2, 3), probably due to the occurrence of the reverse water–gas shift reaction (Eq. 2) consuming the CO_2 and producing water.

Comparing the CH_4 conversions in the DRM and SRM reactions, it is found that the conversions are higher in the SRM reaction which may be related to the presence of much lower amounts of carbon in the SRM reaction because of the water injection to the system instead of CO_2. Furthermore, comparing the maximum CH_4 conversions in the DRM and SRM processes illustrates almost 92 and 97 % conversions, respectively, using GHSV = 10,500 h^{-1} at 800 °C reflecting higher efficiency of the SRM reaction.

It was pointed out that the steam reforming reaction was occurred at the metal–support interface through the reaction between the water preferentially adsorbed on the support (which allowed the mobility of oxygen species originated from water dissociation on the surface) and the methane preferably adsorbed on the metal (Carvalho et al. 2009). Furthermore, it was noted that by increasing water adsorption-dissociation rate on the catalyst, coke formation was stopped.

In the DRM reaction, the H_2/CO ratio increases with temperature enhancement (Fig. 2). The H_2/CO ratio is 0.387 at 500 °C while it is 0.855 at 800 °C using feed WHSV = 3 L/h. All of the H_2/CO ratios are smaller than unity in the DRM reaction and this can be due to the reverse water–gas shift reaction (Eq. 2). The H_2/CO ratio is decreased from 500 to 800 °C in the SRM reaction (Fig. 3) so that it is 55.76 at 500 °C using feed WHSV = 3 L/h but it is reduced to 5.86 at 800 °C. This is owing to higher consumption of H_2 through the reverse water–gas shift reaction (Eq. 2) at higher temperatures.

An appropriate reforming catalyst must be stable for an extended period of time on stream (TOS) during methane conversion. Therefore, the nanocatalyst was tested for a period of 30 h on stream in the DRM and SRM reactions. The performance of the 3 %Ru/$CeZr_{0.5}GdO_4$ catalyst was evaluated at a constant GHSV = 10,500 h^{-1}, $T = 700$ °C and the results are indicated in Fig. 4. Interestingly, it is seen that the CH_4 conversions are almost constant within 30 h of the DRM and SRM reactions reflecting the catalyst extraordinary stability with time (absence of coke formation or sintering). The CH_4 and CO_2 conversions are also slightly increased in the DRM process. Furthermore, in the DRM reaction, the CH_4 conversions are lower than their related CO_2 conversion that can be attributed to the reverse water–gas shift reaction (Eq. 2). It is seen that very much higher CH_4 conversions are obtained in the SRM than in the DRM indicating higher efficiency of the SRM process.

The most important and valuable result in these figures is the completely constant catalytic activity and catalyst stability within the 30 h time on stream experiments that was not observed for the common 10 %Ni/γ-Al_2O_3 catalyst (Yang et al. 2010). These findings support that the tested 3 %Ru/$CeZr_{0.5}GdO_4$ catalyst is an extremely suitable and stable candidate for the reforming reactions to achieve very high conversions and yields especially in the SRM process.

A possible reason for the high catalytic activity and stability of the 3 %Ru/$CeZr_{0.5}GdO_4$ catalyst is that the

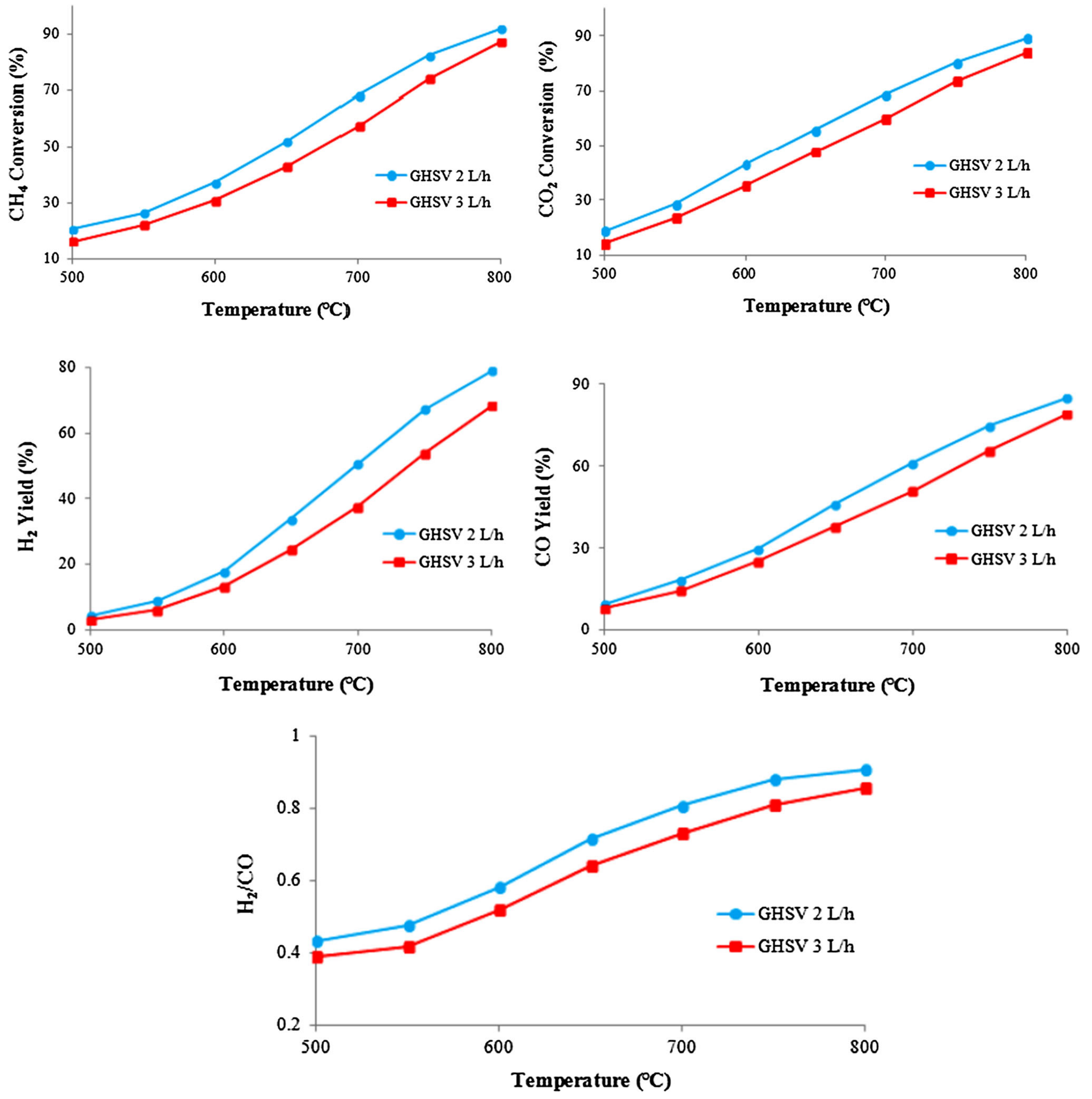

Fig. 2 CH_4, CO_2 conversions, CO, H_2 yields and H_2/CO ratio in the DRM reaction with feed WHSV = 2, 3 L/h using the 3 %Ru/$CeZr_{0.5}GdO_4$ catalyst

support acidic sites consume ruthenium electrons to reduce the acidity of the support, thereby affect/increase catalytic activity of the catalyst for methane conversion (Carvalho et al. 2009).

The catalysts supported on ceria-containing materials for CH_4 reforming reactions have attracted attention due to their high oxygen storage capacities (Chen et al. 2010). The mechanism of CH_4–CO_2 reforming over Ru-based catalysts has been widely investigated (Matsui et al. 1999), and it was proposed that the CH_4 and CO_2 are adsorbed and dissociated on the transition metal surface. The adsorbed CH_x $(0 < x < 3)$ species and H_2 originate from the dissociation of CH_4, while the adsorbed oxygen species and CO are from the dissociation of CO_2. The oxygen species react with the CH_x species to produce CO and H_2. The support also contributes in the reaction. It is well known that Ce-based materials take part in the activation of CH_4 and CO_2 through reactions (15)–(17) when they are used as the

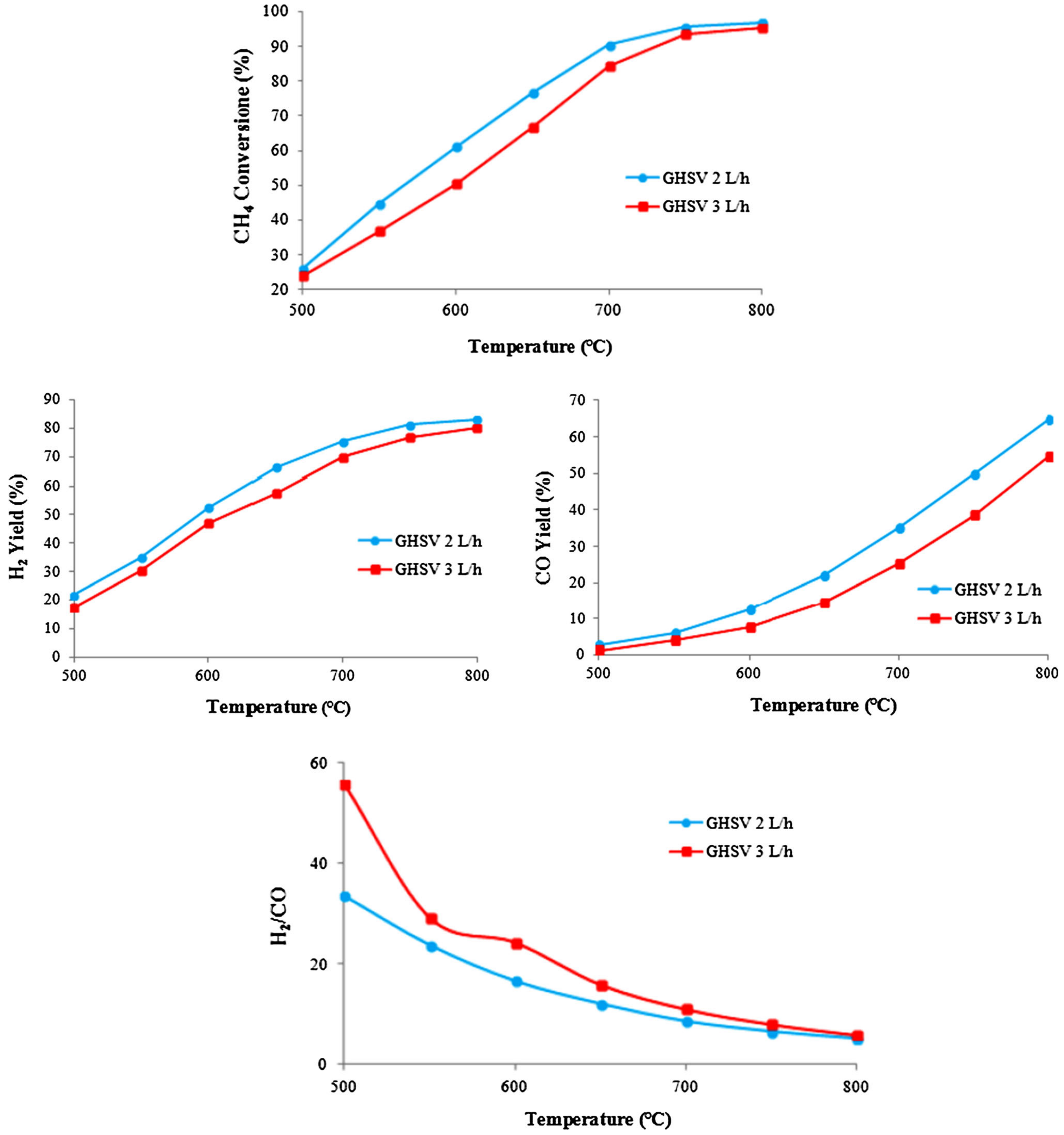

Fig. 3 CH_4 conversion, CO, H_2 yields and H_2/CO ratio in the SRM reaction with feed WHSV = 2, 3 L/h using the 3 %Ru/$CeZr_{0.5}GdO_4$ catalyst

supports or promoters. The same case may happen for our $CeZr_{0.5}GdO_4$-supported Ru catalyst.

$$CeO_2 + nCH_4 \rightarrow CeO_{2-n} + nCO + 2n\,H_2 \tag{15}$$

$$CeO_2 + nH_2 \rightarrow CeO_{2-n} + nH_2O \tag{16}$$

$$CeO_{2-n} + nCO_2 \rightarrow CeO_2 + nCO \tag{17}$$

It was indicated that the $Ce_xZr_{1-x}O_2$ solid solutions have high oxygen storage capacities and ceria can store hydrogen (Wu et al. 2008). Thus, $Ce_xZr_{1-x}O_2$ solid solutions supported Ru catalysts revealed excellent performance in CH_4–CO_2 reforming. Also, it was reported that in order to overcome the rather low thermal

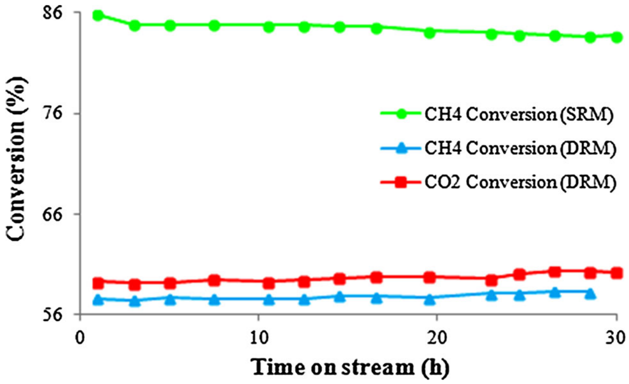

Fig. 4 CH_4 and CO_2 conversions after 30 h time on stream (TOS) with a feed WHSV = 3 L/h at 700 °C in the DRM and SRM reactions using the 3 %Ru/CeZr$_{0.5}$GdO$_4$ catalyst

stability of ceria, zirconia (ZrO_2) was added to ceria to form a solid solution and thus improve its thermal stability (Aw et al. 2014). The advantages of zirconia are based on its good affinity to CO_2 adsorption for DRM and its excellent thermal stability (Mustu et al. 2013). Accordingly, our 3 %Ru/CeZr$_{0.5}$GdO$_4$ catalyst that has a high performance and resistance to carbon deposition may act by the above-mentioned mechanism.

Evaluations of the used nanocatalysts in the reforming reactions

In order to evaluate the coke formation and its amount on the used 3 %Ru/CeZr$_{0.5}$GdO$_4$ nanocatalyst (30 h in the dry and steam reforming conditions at 700 °C and atmospheric pressure), the TGA/DTA analysis was performed. The results are displayed in Fig. 5a, b. It is obvious from both curves that the coke formation was not happened on none of the catalysts used in the DRM and SRM processes.

Interestingly, the TGA diagrams revealed 1.41 and 0.97 % increase in the weights of catalysts used in the DRM and SRM reactions. Also, it is observed that the maximum increase in the catalysts weights is occurred above 600 °C. The increase in the catalysts weights can be due to the entrapment of gaseous feeds within the catalysts pores because after the temperature is raised above 600 °C, an increase in the catalyst volume is practically seen that is almost three times greater than its original volume.

It can be stated that, to the best of our knowledge, the absence of coke formation on our 3 %Ru/CeZr$_{0.5}$GdO$_4$ catalyst is not yet observed and it is reported here for the first time. This can be attributed to the effect of both CeZr$_{0.5}$GdO$_4$ support and Ru noble metal that are highly resistant against coke deposition. Indeed, among numerous investigations performed using various catalysts especially noble metals as active catalysts (Djinović et al. 2012; Özkara-Aydınoğlu and Aksoylu 2010), amount of coke formation has only been decreased to low values but it was not vanished completely.

Surprisingly, there are three endothermic peaks at about 140–160, 330 and 640 °C in the DTA diagrams of the catalysts used in the DRM and SRM reactions. Since there is not any small amount of carbon deposit on each catalyst, the three peaks are indicative of endothermic nature of gas adsorption within the pores of catalyst particles. Indeed, this is an extraordinarily desirable result for the novel catalyst prepared here, and as anticipated, the 3 %Ru/CeZr$_{0.5}$GdO$_4$ sample acts as a very stable catalyst during 30 h time on stream in both the DRM and SRM processes.

In order to confirm the absence of the coke formation on our 3 %Ru/CeZr$_{0.5}$GdO$_4$ catalyst used in the DRM and SRM reactions, their FE-SEM images were prepared (Fig. 5c, d). It is obviously observed that there are not any quantities of coke on the catalysts applied in both the DRM and SRM reactions. This result confirms the TGA/DTA analysis in the above section. Moreover, it is seen that the catalysts have almost maintained their sheet-like morphologies and fine dispersion after being used in the DRM and SRM processes.

Comparing these results with that obtained from the TPR analysis in which the 3 %Ru/CeZr$_{0.5}$GdO$_4$ nanocatalyst has a low onset reduction temperature justifies that the convenient reduction of the catalyst can modify its support–metal interaction, thus inhibit the agglomeration of catalyst particles and prevent carbon deposition on its surface.

The FT-IR spectra of the CeZr$_{0.5}$GdO$_4$ support and 3 %Ru/CeZr$_{0.5}$GdO$_4$ catalyst used in the DRM and SRM reactions are demonstrated in Fig. S3. It is observed that the intensities of bands are approximately identical for the fresh and the used catalysts. However, the band intensities are the lowest for the fresh catalyst than those of the used catalysts. This can be attributed to the entrapment of gaseous feeds within the catalysts pores which is greater for the catalyst applied in the DRM than in the SRM process probably due to using a feed with higher carbon content ($CO_2 + CH_4$) in the DRM than in the SRM reaction ($H_2O + CH_4$). This result is in excellent consistence with the results obtained from the TGA/DTA and FE-SEM analyses.

The broadbands around 3400 cm^{-1} in the FT-IR spectra are attributed to the OH stretching frequency that can also be related to the adsorption of water molecules produced during the reverse water–gas shift reaction (Eq. 2)

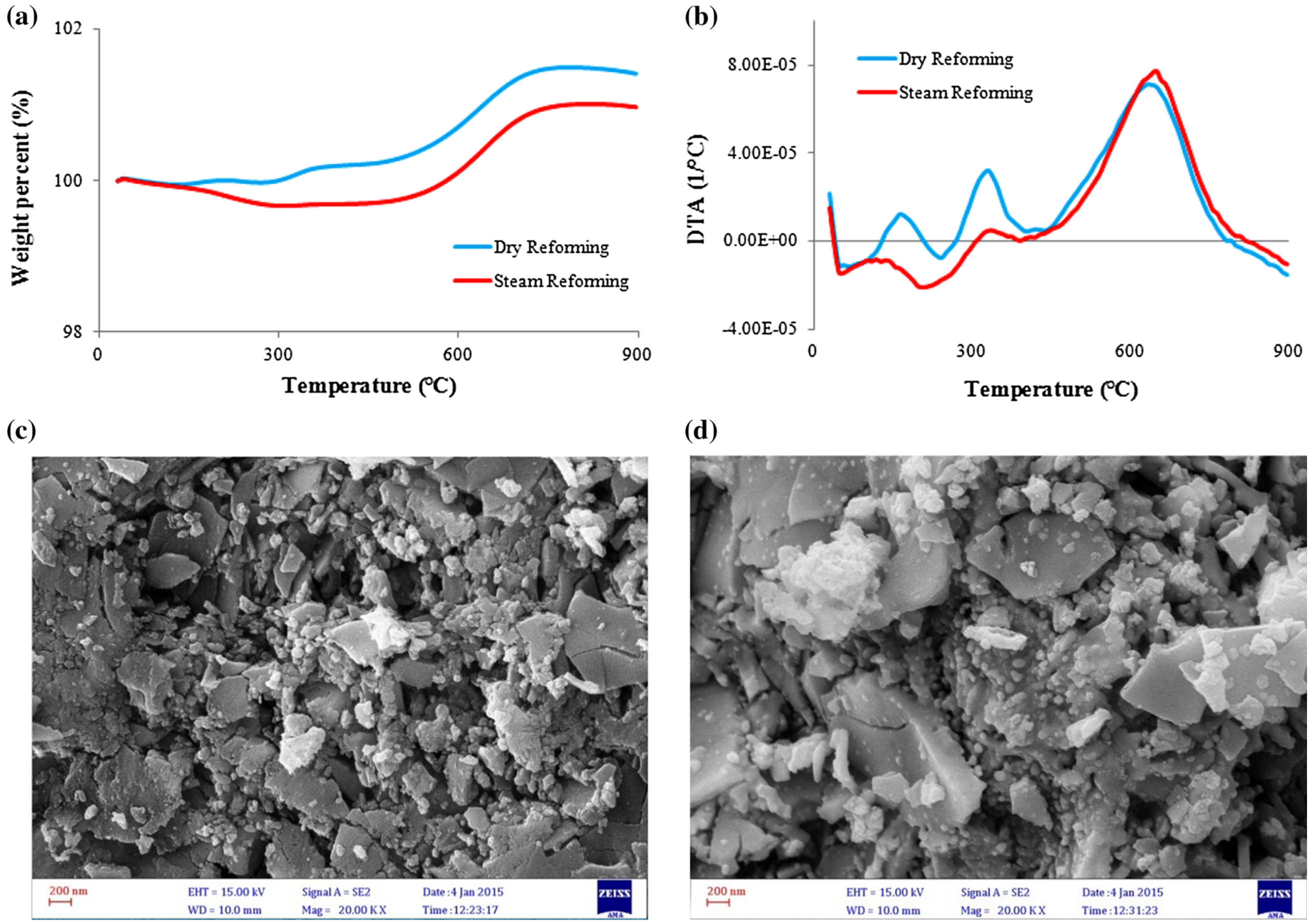

Fig. 5 TGA (**a**) and DTA (**b**) curves for the 3 %Ru/CeZr$_{0.5}$GdO$_4$ used catalyst in the DRM and SRM reactions. The FE-SEM micrographs of 3 %Ru/CeZr$_{0.5}$GdO$_4$ used catalyst in the (**c**) DRM and (**d**) SRM reactions

(Bachiller-Baeza et al. 2013). The spectra exhibit some bands between 1400 and 1700 cm^{-1} pointing to the presence of carbonate species. The origin of the carbonaceous compounds can be the CO and CO$_2$ gasses. The bands appeared at about 420 and 580 cm^{-1} are assigned to the metal-oxide stretching frequencies.

Conclusion

The catalytic conversion of methane in the DRM and SRM reactions was investigated under various conditions including $P = 1$ atm, seven temperatures ($T =$ 500–800 °C) and two GHSVs = 7000, 10,500 h^{-1}. For this purpose, a new 3 %Ru/CeZr$_{0.5}$GdO$_4$ nanocatalyst was synthesized and applied as an efficient sample in the DRM and SRM reactions. The TPR profile of the 3 %Ru/CeZr$_{0.5}$GdO$_4$ catalyst exhibited a low onset reduction temperature at 183.21 °C that can be attributed to the high oxygen mobility on the catalyst surface. Surprisingly, the TGA/DTA analyses did not reveal any coke deposits on both the catalysts used in the DRM and SRM reactions and this fact was supported by the FE-SEM images. Moreover, the increase in the weight of catalysts observed in the TGA graphs was probably due to the entrapment of gaseous feeds within the catalysts pores. The CH$_4$ and CO$_2$ conversions were all almost constant within 30 h time of the DRM and SRM reactions reflecting the catalyst extraordinary stability with time, absence of coke formation or sintering of the catalyst. Also, the relatively low H$_2$O/CH$_4$ ratio of 3 used in the SRM reaction confirms the high catalytic activity of the catalyst. Therefore, in comparison with other catalysts reported in literature, our new 3 %Ru/CeZr$_{0.5}$GdO$_4$ nanocatalyst is a superior candidate for application in the DRM and SRM reactions due to its very higher stability with time, totally resistance against coke formation (which was not seen at all for similar related catalysts in literature), low reduction temperature (easy regeneration) and high conversions/yields.

Acknowledgments The authors wish to appreciate all who have assisted in conduction of this work.

References

Aw MS, Osojnik Črnivec IG, Djinović P, Pintar A (2014) Strategies to enhance dry reforming of methane: synthesis of ceria-zirconia/nickel–cobalt catalysts by freeze-drying and NO calcinations. Int J Hydrogen Energy 39:12636–12647

Bachiller-Baeza B, Mateos-Pedrero C, Soria MA, Guerrero-Ruiz A, Rodemerck U, Rodríguez-Ramos I (2013) Transient studies of low-temperature dry reforming of methane over Ni–CaO/ZrO_2–La_2O_3. Appl Catal B Environ 129:450–459

Bakkerud PK (2005) Update on synthesis gas production for GTL. Catal Today 106:30–33

Barroso-Quiroga MM, Castro-Luna AE (2010) Catalytic activity and effect of modifiers on Ni-based catalysts for the dry reforming of methane. Int J Hydrogen Energy 35:6052–6056

Bermúdez JM, Fidalgo B, Arenillas A, Menéndez JA (2012) CO_2 reforming of coke oven gas over a Ni/γAl_2O_3 catalyst to produce syngas for methanol synthesis. Fuel 94:197–203

Carvalho LS, Martins AR, Reyes P, Oportus M, Albonoz A, Vicentini V, Rangel MC (2009) Preparation and characterization of Ru/MgO–Al_2O_3 catalysts for methane steam reforming. Catal Today 142:52–60

Chen J, Yao C, Zhao Y, Jia P (2010) Synthesis gas production from dry reforming of methane over $Ce_{0.75}Zr_{0.25}O_2$-supported Ru catalysts. Int J Hydrogen Energy 35:1630–1642

Djinović P, Batista J, Pintar A (2012) Efficient catalytic abatement of greenhouse gases: methane reforming with CO_2 using a novel and thermally stable Rh–CeO_2 catalyst. Int J Hydrogen Energy 37:2699–2707

Jakobsen JG, Jørgensen TL, Chorkendorff I, Sehested J (2010) Steam and CO_2 reforming of methane over a Ru/ZrO_2 catalyst. Appl Catal A: Gen 377:158–166

Jones G, Jakobsen JG, Shim SS, Kleis J, Andersson MP, Rossmeisl J, Abild-Pedersen F, Bligaard T, Helveg S, Hinnemann B, Rostrup-Nielsen JR, Chorkendorff I, Sehested J, Nørskov JK (2008) First principles calculations and experimental insight into methane steam reforming over transition metal catalysts. J Catal 259:147–160

Klug HP, Alexander LE (1954) X-ray diffraction procedure. Wiley InterScience, New York, pp 504–524

Kohn MP, Castaldi MJ, Farrauto RJ (2014) Biogas reforming for syngas production: the effect of methyl chloride. Appl Catal B Environ 144:353–361

Levy M, Levitan R, Meirovitch E, Segal A, Rosin H, Rubin R (1992) Chemical reactions in a solar furnace 2: direct heating of a vertical reactor in an insulated receiver. Experiments and computer simulations. Sol Energy 48:395–402

Lucredio AF, Assaf JM, Assaf EM (2012) Reforming of a model biogas on Ni and Rh–Ni catalysts: effect of adding La. Fuel Process Technol 102:124–131

Luna AEC, Iriarte ME (2008) Carbon dioxide reforming of methane over a metal modified Ni–Al_2O_3 catalyst. Appl Catal A Gen 343:10–15

Lunsford JH (2000) Catalytic conversion of methane to more useful chemicals and fuels: a challenge for the 21st century. Catal Today 63:165–174

Matsui N, Anzai K, Akamatsu N, Nakagawa K, Ikenaga N, Suzuki T (1999) Reaction mechanisms of carbon dioxide reforming of methane with Ru-loaded lanthanum oxide catalyst. Appl Catal A 179:247–256

Mustu H, Arbag H, Yasyerli S, Yasyerli N, Dogu G, Dogu T (2013) Mesoporous zirconia supported nickel catalysts for coke minimization in dry reforming of methane. In: Nanotechnology 2013: advanced materials, CNTs, particles, films and composites, vol 1, pp 463–466

Oyama ST, Hacarlioglu P, Gu Y, Lee D (2012) Dry reforming of methane has no future for hydrogen production: comparison with steam reforming at high pressure in standard and membrane reactors. Int J Hydrog Energy 37:10444–10450

Özkara-Aydınoğlu Ş, Aksoylu AE (2010) Carbon dioxide reforming of methane over Co–X/ZrO_2 catalysts (X = La, Ce, Mn, Mg, K). Catal Commun 11:1165–1170

Quek X-Y, Liu D, Cheo W, Wang H, Chen Y, Yang Y (2010) Nickel-grafted TUD-1 mesoporous catalysts for carbon dioxide reforming of methane. Appl Catal B 95:374–382

Rostrup-Nielsen JR, Hansen J-HB (1993) CO_2-Reforming of methane over transition metals. J Catal 144:38–49

Roy PS, Park N-K, Kim K (2014) Metal foam-supported Pd–Rh catalyst for steam methane reforming and its application to SOFC fuel processing. Int J Hydrogen Energy 39:4299–4310

Sun GB, Hidajat K, Wu XS, Kawi S (2008) A crucial role of surface oxygen mobility on nanocrystalline Y_2O_3 support for oxidative steam reforming of ethanol to hydrogen over Ni/Y_2O_3 catalysts. Appl Catal B 81:303–312

Sutthiumporn K, Kawi S (2011) Promotional effect of alkaline earth over Ni–La_2O_3 catalyst for CO_2 reforming of CH_4: role of surface oxygen species on H_2 production and carbon suppression. Int J Hydrogen Energy 36:14435–14446

Wei JM, Iglesia E (2004) Mechanism and site requirements for activation and chemical conversion of methane on supported pt clusters and turnover rate comparisons among noble metals. J Phys Chem B 108:4094–4103

Wu X, Kawi S (2009) Rh/Ce–SBA-15: active and stable catalyst for CO_2 reforming of ethanol to hydrogen. Catal Today 148:251–259

Wu QY, Chen JX, Zhang JY (2008) Effect of yttrium and praseodymium on properties of $Ce_{0.75}Zr_{0.25}O_2$ solid solution for CH_4–CO_2 reforming. Fuel Process Technol 89:993–999

Wurzel T, Malcus S, Mleczko L (2000) Reaction engineering investigations of CO_2 reforming in a fluidized-bed reactor. Chem Eng Sci 55:3955–3966

Yang R, Xing C, Lv C, Shi L, Tsubaki N (2010) Promotional effect of La_2O_3 and CeO_2 on Ni/γ–Al_2O_3 catalysts for CO_2 reforming of CH_4. Appl Catal A Gen 385:92–100

Zhai X, Ding S, Liu Z, Jin Y, Cheng Y (2011) Catalytic performance of Ni catalysts for steam reforming of methane at high space velocity. Int J Hydrogen Energy 36:482–489